Influence of Polymer Motion, Topology and Simulation Size on Penetrant Diffusion in Amorphous, Glassy Polymers: Diffusion of Helium in Polypropylene

Jan H. D. Boshoff,[†] Raul F. Lobo,[‡] and Norman J. Wagner*[,†]

Center for Molecular and Engineering Thermodynamics and Center for Catalytic Science and Technology, Department of Chemical Engineering, University of Delaware, Newark, Delaware 19716

Received February 12, 2001; Revised Manuscript Received May 18, 2001

ABSTRACT: The influence of polymer topology and motion on the diffusion of a small gas penetrant (He) in united atom atactic polypropylene models of varying density (0.872−0.971 g/cm^3) and simulation cell size (27−60 Å), are studied by performing molecular dynamics simulations on rigid polymer structures. A multimode analysis of the self-part of the van Hove space−time autocorrelation function for penetrant diffusion is introduced to investigate the mechanism of diffusion and distinguish simulation box size effects. For the frozen matrix, the diffusion is no longer an activated process but is better described as hindered kinetic motion. The anomalous diffusion regime is identified to be a consequence of the tortuosity in the percolated diffusion pathways in the polymer structure, which itself is connected to the correlation length in the polymer glass. Comparisons with fully mobile matrix simulations demonstrate the influence of polymer motion on the mechanism of molecular diffusion in glassy polymers and are in qualitative agreement with previous studies. The turnover from anomalous to Fickian diffusion shows a marked simulation size dependence not seen in the results for which the polymer is allowed thermal motion.

1. Introduction

The method of molecular dynamics (MD) has been successfully applied to study diffusion of small penetrants in amorphous polymers.[1,2] The usefulness of MD becomes apparent in the amount of detail that can be obtained in studying penetrant diffusion. In almost all instances, the goal of molecular simulation is not necessarily to calculate the exact diffusivities of specific penetrants in specific polymers, but rather the study of the effects of polymer structure, chemical composition, and structure dynamics on the mechanism of penetrant diffusion on an atomistic level.[1−8] However, the largely qualitative nature of tractable MD simulations involving polymers[1] and a lack of predictive engineering models for permeation in glassy polymers hinder the rational design of novel barrier materials from first principles.

Coupling of the penetrant motion to local or segmental polymer motion is known to influence the rate of diffusion of gas molecules in amorphous polymers.[9−11] Previous studies have shown that penetrant motion exhibits a region of anomalous diffusion between short-time ballistic and long-time Fickian diffusion. This region is attributed to the tortuous pathway topology and correlated motion in the polymeric structure in which the penetrants diffuse.[1] The exact influence of each of these effects and methods to model them analytically have not yet been established. Polymer motion is known to aid penetrant diffusion in the dynamic formation of cavities between which jump events occur, leading to a diffusion mechanism that is generally thought of to be an activated process.[1] The polymer structure also plays an important role in the rate process, as it will determine the local structure of activation barriers, as well as the available pathways for diffusion. Transition state theory simulations have shown[12,13] that the majority of penetrant jump events occur in the vicinity of the polymer side groups, due to the relative mobility of the side groups compared to the chain backbone. As a result, correlated motion of the penetrant and polymer side groups must be considered in calculating activation barriers. The characteristic time scales of motion of the polymer side groups are comparable to that of the penetrant but are much shorter than the time scale required for backbone rearrangement.

The turnover from anomalous to Fickian diffusion is also known to depend on the simulation's periodic box size,[5,14] which can lead to erroneous calculations of the diffusivity. If the dimension of the periodic image is sufficiently small, such that Fickian diffusion is not achieved before the penetrant samples multiple periodic boxes, random motion is artificially induced, leading to erroneous results. Local polymer motion has been shown to diminish this effect[5] because fluctuations in the polymer are sufficient to significantly alter the matrix before the penetrant samples multiple periodic images. Questions remain, however, on the precise influence of polymer topology and local thermal motion on the regime of anomalous diffusion.

The goal of this work is to determine the effects of matrix topology and polymer fluctuations on the mechanism of penetrant diffusion in glassy amorphous polymers. Specifically, the effects of the polymer topology and motion on the molecular diffusion of small molecule penetrants in atactic, glassy polypropylene are decoupled by studying diffusion in "frozen" polymer matrices with MD. This simplified ensemble also permits studying the effects of simulation size on the turnover from anomalous to Fickian diffusion, and the subsequent effects on the calculated diffusivity and solubility on a broader range of sizes than previously explored. A method is proposed for estimating the diffusivities of slow diffusing penetrants in amorphous materials by decoupling "trapped" and diffusing pen-

* Corresponding author. E-mail: wagner@che.udel.edu.
[†] Center for Molecular and Engineering Thermodynamics, Department of Chemical Engineering, University of Delaware.
[‡] Center for Catalytic Science and Technology, Department of Chemical Engineering, University of Delaware.

10.1021/ma010255c CCC: $20.00
Published on Web 07/14/2001

Table 1. Properties of Polymer Structures Used in the Simulations

density, g/cm^3	lattice size	box dimens, Å	chain length monomers	mol wt	methane molecules
0.872	5 × 5 × 5	27.145	250	10 500	25
0.872	7 × 7 × 7	38.003	686	28 812	69
0.878	9 × 9 × 9	48.744	1458	61 236	135
0.872	11 × 11 × 11	59.719	2662	111 804	195
0.892	7 × 7 × 7	37.065	651	27 342	49
0.910	7 × 7 × 7	36.330	626	26 292	37
0.934	7 × 7 × 7	35.553	602	25 284	21
0.955	7 × 7 × 7	34.804	577	24 234	7
0.971	7 × 7 × 7	34.083	551	23 142	0

Table 2. Lennard-Jones Parameters Employed in the Simulations

molecule	ϵ, kJ/mol	σ, Å
UA CH_1	0.377	3.296
UA CH_2	0.502	3.430
UA CH_3	0.628	3.564
UA CH_4	1.230	3.813
He	0.085	2.580

etrants through analysis of the self-part of the Van-Hove space−time autocorrelation function.

2. Simulation Methods

A. Simulation Model. The polymer model considered in this work is glassy, atactic polypropylene. Amorphous polymer structures were created by means of a stochastic lattice algorithm,[8] which has been previously employed and validated to generate the proper chain statistics[1] of the lattice backbone. The backbone was then decorated and annealed according to a procedure described elsewhere.[5,6] Briefly, a Monte Carlo (MC) algorithm is used to generate a sequence of candidate polymer configurations on a lattice that satisfy the periodic boundary constraints with a Gaussian backbone topology on all relevant length scales. In addition to exhibiting Gaussian chain statistics, the chain also packs properly into a periodic simulation cell. This lattice topology is decorated with atomistic (united atom) atactic polypropylene and annealed for 200 ps at 1000 K and then for 300 ps at 233 K to generate candidate structures. All simulations here correspond to a single backbone chain replicated in space to create the polymer glass. The force field expressions and parameters for the bond stretching and bending, torsion angle rotation and nonbonded interactions were obtained from AMBER.[15] The MD simulations for annealing of the polymer structures were performed using a time step of 0.002 ps, using the MD simulation package AMBER 4.1.[16] To prevent a nonuniform distribution of void volume in the lower density structures (i.e., "cracking" of the polymer), the lower density polymer structures were dissolved in a small amount of methane, with sufficient methane molecules added to ensure the same void volume fraction as the highest density polymer ($f^{\text{void}} = 0.392$ based on van der Waals radii of polymer atoms). After annealing, the methane was removed. Table 1 gives a summary of the polymer structures generated for this work, where five statistically independent structures were created for each of the densities listed in Table 1. Methane was modeled as a united atom sphere. All the Lennard-Jones parameters are given in Table 2. The equilibrium C−C bond length in the structures is 1.53 Å.

The structures were quenched to $T = 0$ K after equilibration and used directly in all of the subsequent studies. Freezing the polymer motion decouples the effects of polymer dynamics and structure on the diffusion behavior of small penetrants. Alternatively, it is an approximation of the limit of the glassy phase of the polymer structures[17] in that the polymer undergoes no structural rearrangement on the time scales of observation.

Molecular dynamics simulations using the standard leapfrog algorithm to solve the equations of motion were performed on the penetrant atoms within frozen polypropylene structures. The polymer model was a united atom polypropylene with nonbonded Lennard-Jones potential parameters, which are summarized in Table 2. An excluded volume map (EVM) of each polymer structure was created by inserting helium atoms on a grid of 0.2 Å. Twenty five helium atoms were inserted into randomly selected energetically favorable positions according to the EVM. The helium atoms were not allowed to interact with one another in order to measure the diffusive behavior in the dilute limit. Each He atom, together with the polymer matrix, represents an *NVE* system with collisions between the He atom and the matrix completely elastic. Once the potential energy pathway of the penetrant is established, the kinetic energy will fluctuate within the initial temp window. The 25 He atoms with polymer matrices were considered to be an *NVE* ensemble, with He atoms assigned a Maxwell−Boltzmann distribution of velocities with average around the desired temp of 233 K. During the first 20 ps the system of 25 He atoms was equilibrated with a velocity rescaling algorithm[18] to thermalize the He at 233 ± 20 K. This was found to be sufficient time for the potential and kinetic energy to reach a steady-state value. After thermal annealing of the penetrants, the thermostat was turned off and the kinetic energy remained stable (to within 18 K) for the remainder of the run duration (up to 10 ns) without any further velocity rescaling. The Maxwell−Boltzmann velocity distribution was verified to be accurately maintained throughout the course of the run. All calculations are based on simulation runs of 10 ns with a time step of 0.005 ps.

B. Polymer Structure Characterization. Creating polymer structures that are representative of the bulk material is a crucial step in simulation studies.[1,8,19−22] Several characterization techniques were employed to ensure that the polymer structures were sufficiently representative of bulk amorphous polypropylene. The chain statistics of the lattice backbones were observed to follow Gaussian statistics, as generated by the algorithm of Kotelyanskii et al.[8] Plots of the mean squared distance between lattice points ($\log(\langle r^2 \rangle)$) vs the number of lattice segments between the two points under consideration ($\log(n)$) yielded excellent agreement with the expected relationship $\langle r^2 \rangle = 1.5nl^2$, with l the lattice size and n the number of segments.

The elastic X-ray structure factor, $S(q)$ was approximated by integration of the total radial distribution function, according to eq 1

$$S(q) = 1 + \frac{2}{V}\frac{(N_A - 1)}{2}\int 4\pi r^2[g(r) - 1]\frac{\sin(rq)}{rq}\mathrm{d}r \quad (1)$$

where q is the scattering vector defined by

$$q = \frac{4\pi}{\lambda}\sin\theta \quad (2)$$

The phase difference between two scattered photons is expressed by rq and N_A is the total number of scattering

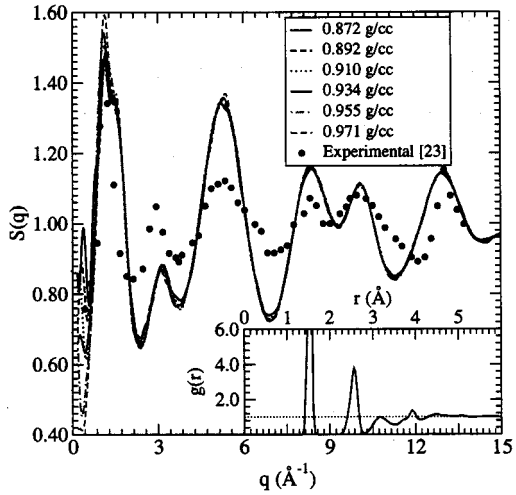

Figure 1. Average elastic X-ray structure factor for all samples considered in this study, compared to experimental values.[23] The inlay shows a typical radial pair distribution function, indicating the extent of correlation in the polymer structures.

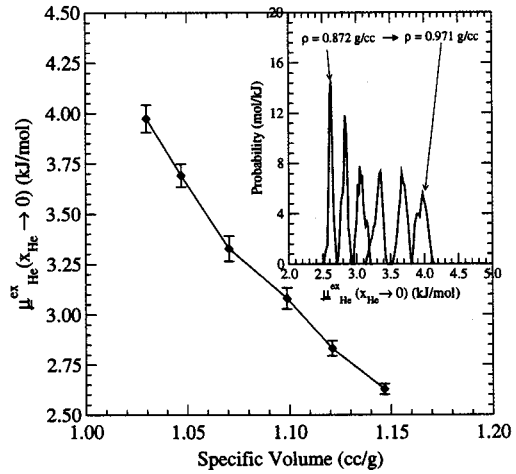

Figure 2. Calculated excess chemical potential of He in the polymer structures based on the 7 × 7 × 7 lattice backbone as a function of specific volume. The inlay shows the distributions of the excess chemical potentials as a function of the specific volume.

centers in the sample volume *V*. In writing eq 1, it is assumed that the three carbon scattering centers present in polypropylene are identical. Figure 1 compares the average calculated structure factor as a function of the density for all the structures considered in this study with experimental results.[23] The calculated structure factors are in semiqualitative agreement with experimental results for the model considered in this work. The differences are ascribed to a deviation from the expected torsional angle distribution as predicted using rotational isomeric-state (RIS) theory.[19] During structure annealing at high temperatures, the torsional angles are randomized and trapped in this distribution upon a sudden quench to 233 K. At 233 K, the thermal energy is insufficient for significant gauche−trans translations to restore the proper torsional angle distribution[19] within the annealing time (300 ps). The inlay in Figure 1 shows the total radial distribution function for a 0.892 g/cm^3 structure, which is representative of all the structures considered in this work. For all the structures considered, correlation in the radial distribution function decays to 1.000 ± 0.025 within ≈5.4 Å and 1.000 ± 0.005 within ≈11.0 Å. The lengths $l_{c1} = 2(5.4)$ = 10.8 Å and $l_{c2} = 2(11.0) = 22.0$ Å are characteristic of correlation lengths in the polymer structures.

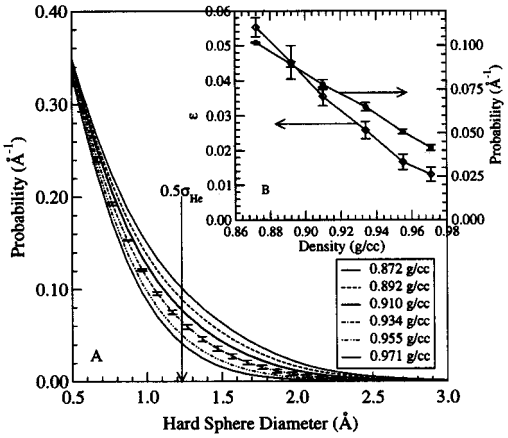

Figure 3. (A) Cavity size distributions by probing with a hard sphere of radius *r*. Arrow indicates probabilities at $r = \sigma_{He}/2$. The error bars on the 0.934 g/cm^3 line are representative of the standard deviation found in all the data presented on the graph. (B) Polymer structure porosity as a function of density (◇) and the probability density corresponding to a spherical cavity the size of He (●). The similar linear dependence on density of both these parameters show that the void volume is distributed homogeneously in the polymer structures (i.e., no "cracking").

Another property that is sensitive to simulation size effects is the calculated solubility of a gas in the polymer. This can be estimated from the excess chemical potential at infinite dilution of the solute in the polymer, which is calculated using Widom's test particle insertion method and variations thereof.[6,24,25] In this work the approach explained by Cuthbert et al.[6] was followed. First, an excluded volume map of the structure is constructed. The excess chemical potential is calculated by probing the polymer structure on a grid of 0.3 Å with a hard sphere two-thirds the size of He to determine the excluded volume map. A He atom is then inserted into the open sites, and the change in potential energy calculated via the method described by Cuthbert et al.[6] Results are shown in Figure 2, representing excess chemical potentials calculated from the last 100 ps of annealing of the polymer structures. The results in Figure 2 indicate that in the infinite dilution limit, the favorable interaction between He and the polymer leads to an increase in excess chemical potential with polymer density. A qualitative interpretation of this is as the polymer densifies, the smaller cavities offer on average more attractive interactions with the small penetrant. The inlay in Figure 2 shows the distribution of calculated excess chemical potential as a function of the density in the structures, smoothed to account for the finite bin size. The distributions are comparable for all the structures, showing no anomalous behavior with polymer density.

The cavity size distribution can be estimated by means of a hard sphere insertion procedure similar to that mentioned above for calculating the solubility. A grid of 0.1 Å was placed on each of the simulation boxes and probed with hard spheres of variable radii. This result in the probability distributions shown in Figure 3A. The graph indicates the average probability distribution for finding a spherical cavity of radius *r* in the polymer structures, i.e., a spherical cavity size distribution, as a function of density. The vertical arrow on the graph indicates the Lennard-Jones radius of He used

in the simulation. There is a linear dependence of the probability of finding a cavity the size of He on the polymer density, as shown in Figure 3B.

The porosity of the structures was also estimated from the hard sphere insertion probability of a sphere of radius $\sigma_{He}/2$. The ratio of successful insertions to total attempts represents the fractional volume occupiable by He, and is plotted as porosity in Figure 3B. This porosity depends linearly on the density with values ranging between 1.2% and 5.5%. The congruence of the cavity size distribution and the porosity, as plotted in Figure 3B, shows that there is no anomalous dependence of the void volume distribution on the density, i.e., no "cracking" in the structures.

C. Analysis of MD Results. Tracer diffusivity can be determined from the calculated mean-squared displacement (MSD) of the penetrants by fitting the Einstein equation to the long time limit of the MSD:

$$\langle r^2(t)\rangle = \lim_{ct\to\infty} 6D_{MSD}\, t \tag{3}$$

The region used to calculate the diffusivity was determined by examining the slope of the MSD on a log−log scale. The Fickian diffusive regime was defined to be when the slope of the MSD remained within 10% of 1.00.[5] For diffusion in glassy polymers, the MSD curve typically consists of three regions: a short time ballistic regime, with $\langle r^2\rangle \propto t^2$, an anomalous regime on intermediate time scales, where $\langle r^2\rangle \propto t^x$, $x < 1.0$, and finally, Fickian diffusion in the long time limit, when motion is random and $\langle r^2\rangle \propto t$.

The self-part of the van Hove function, $G_s(r, t)$, gives the probability for a penetrant to move a given distance r in a given time t. The benefits of analyzing this space−time autocorrelation function for diffusion results have been shown before.[5,26] In the long time limit, where motion becomes random, the van Hove function for a population of penetrants can be described by a Gaussian distribution about the average distance diffused:

$$G_s(r, t) = (4D_{vH}t)^{-3/2} e^{-r^2/4D_{vH}t} \tag{4}$$

In eq 4 D_{vH} is the Fickian diffusivity, obtained by fitting the measured self-part of the van Hove function to the expression above and is expected to be equal to D_{MSD} in the long time limit.

Diffusants in tortuous structures, such as glassy polymers, move in a highly nonrandom fashion at short and intermediate time scales, leading to van Hove functions that deviate from the Gaussian limit described by eq 4. To account for the non-Gaussian behavior, the van Hove function is empirically modeled as the linear sum over independently diffusing populations. If it is assumed that the diffusing population can be divided into a number of independent samples, each diffusing with a distinct diffusivity, the van Hove function will be described by the following function

$$4\pi r^2 G_s(r, t) = 4\pi r^2 \sum_i x_i (4\pi D_i t)^{-3/2} e^{-r^2/4D_i t} \tag{5}$$

where x_i is the fraction of the population diffusing with a diffusivity of D_i. If the diffusion of each fraction is non-Gaussian, eq 5 must be further generalized to allow for each diffusivity D_i to be time-dependent, i.e., $D_i(t)$. If the diffusing population were truly indistinguishable, x_i would relate to the *average* fraction of the population diffusing with an instantaneous diffusivity of D_i. Integration over all displacements yields the average diffusivity as

$$\langle r^2(t)\rangle = \int_0^\infty 4\pi r^2 G_s(r, t) r^2\, dr = 6t\sum_i x_i D_i = 6t/\bar{D}_{vH} \tag{6}$$

The overall diffusivity is seen to be the weighted average of the distinct underlying modes of diffusion. This method enables both defining a measure of the Fickian diffusivity (taken to be $\bar{D}_{vH}$ as $t \to \infty$), as well as identification of the fraction of penetrants that do not diffuse (e.g., due to entrapment). The latter is determined by plotting the average distance diffused $\bar{r}_i(t) = (2/\sqrt{\pi}\sqrt{4D_i t})$by each population as a function of time. The modes that did not diffuse farther than a certain threshold value at a specified time are then taken to be representative of penetrants trapped in the structure. The threshold for the work considered here was taken to be the mean free path of the penetrant atoms, which is calculated as follows: The effect of polymer structure on the diffusivity of the penetrant can be described by macroscopic structural parameters such as the porosity and tortuosity of the polymer matrix. The tortuosity (τ) includes the factors of altering the diffusion path lengths as well as irregularities in the diffusion pathway (i.e., constrictions) and is related to the porosity (ϵ) in the structure by the following relationship[27]

$$\tau = \epsilon \frac{D_k}{D} \tag{7}$$

where D_k is related to the self-diffusion of the penetrant within the "pores" and D is the measured long-time (Fickian) diffusivity.

In the above the term "pore" refers to the molecular diffusion pathways in the amorphous glassy polymer. Although there are no nano- or mesoscale pores identifiable in the dense, amorphous polymers simulated here, we employ the macroscopic concepts of tortuosity and porosity to aid in identifying the molecular mechanisms of diffusion as follows. To implement eq 7, both the porosity ϵ and the short-time diffusivity D_k must be identified. The porosity in the polymer structures considered here is defined as the fractional void volume occupiable to a He atom, as reported in the previous section. We estimated the short-time diffusivity D_k for the helium penetrants using the following equation[28]

$$D_k = {}^1/_3 L_c \bar{v} \tag{8}$$

where L_c is the mean-free path of the penetrant and $\bar{v}$ the average thermal velocity. The velocity autocorrelation function (VACF) were used to estimate the mean-free path of the penetrants in the polymer structures. The VACF for a random walker decays to zero exponentially. However, in the case considered here, the diffusion is "caged" to distances less than that traveled before correlation in the velocity dies away. Collisions with the polymer result in velocity reversal, with the value of $\langle v^{acf}\rangle = 0$ a convenient measure of the average time required for velocity reversal. The mean free path is calculated as $L_c \approx \bar{v}t|_{\langle v^{acf}\rangle=0}$, where t is the average time required for velocity reversal.

3. Results and Discussion

A. Diffusivity. Figure 4 shows the average mean squared displacement of He atoms in the polypropylene

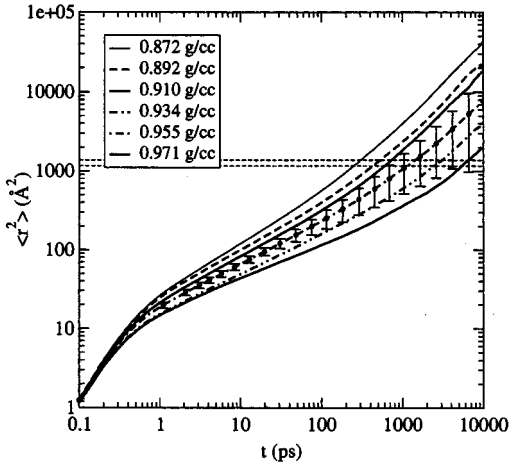

Figure 4. Average mean squared displacement for all He atoms in each of the five polypropylene structures generated from a 7 × 7 × 7 lattice size. Higher density structures limit diffusion due to a reduction in void volume in the polymer structures. The dashed horizontal lines at 1162 and 1374 Å^2 indicate the periodic box length, for the lowest and highest density structures respectively, for reference. The error bars on $\rho = 0.934$ g/cm^3 indicate the typical standard deviation between five independent structures.

Table 3. Diffusivity of He in Polymer Structures As Calculated from Analysis of the MSD's, Where Errors Indicate One Standard Deviation

density, g/cm^3	D, 10^{-5} cm^2/s
0.872	7.64 ± 0.12
0.892	3.71 ± 0.10
0.910	3.32 ± 0.06

structures for structures of varying density. Each curve is an average over five independently generated structures (starting from a 7 × 7 × 7 lattice). The error bars on the 0.934 g/cm^3 line indicate the typical standard deviation between the five different structures. As shown, after the initial ballistic regime ($\langle r^2 \rangle \propto t^2$), there is a broad anomalous regime that scales approximately as $\langle r^2 \rangle \propto t^{0.5}$. At long times the MSD's all tend toward the Fickian limit, where $\langle r^2 \rangle \propto t$. The simulation box size squared is given for reference. The anomalous regime extends to distances comparable to the simulation box size. Increasing the matrix density strongly reduces diffusion in the anomalous and the Fickian regimes. However, the general, qualitative behavior is not altered.

The results obtained for the diffusivity (D_{MSD}) from analysis of the MSD curves of the structures generated from the 7 × 7 × 7 lattice, are shown in Table 3. The highest density at which the diffusivity could be calculated using MSD analysis was 0.910 g/cm^3. Above this density the MSD did not reach Fickian diffusion during the 10 ns of molecular dynamics. Many of the penetrant atoms in the higher density structures are observed to be trapped in the cavities into which they are initially placed on the time scale of the simulation. The lower densities permit faster diffusion due to the higher fraction of void volume.

The regimes of diffusion are clearly identifiable in Figure 5, showing the average derivative of the logarithm of the mean squared displacements, with the time axis on a logarithmic scale. It can be seen from the graph that the Fickian diffusion regime is not reached for the three higher density structures. It is also notable that there is no short-time diffusive regime, which

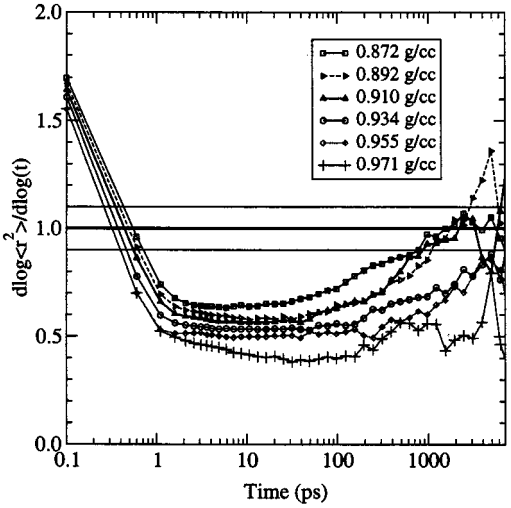

Figure 5. Average derivative of the mean squared displacement of all structures. Fickian diffusion is not reached within the 10 ns of simulation time for the higher density structures.

would be indicated by a value of one at short times. Rather, the motion is ballistic at short times and turns over to the anomalous behavior at intermediate to long time scales. In the anomalous regime, where $\langle r^2 \rangle \propto t^x$, x was found to be $x \cong 0.5$, consistent with earlier results.[14] Interestingly, this dynamic behavior is characteristic of the center of mass diffusion for a reptating polymer chain, which suggests that in the anomalous regime the dynamics of the penetrant is consistent with one-dimensional, tubelike diffusion. This tortuous pathway is established by local correlation in the structure of the polymer. The extent of the anomalous regime is found to be within a factor of 2 of the length scale $l_{c2} = 22.0$ Å, the extent of local correlation in the polymer structure as determined from $g(r)$. As the polymer densifies, the local structure of the polymer backbone determines more of the diffusion pathway, so that the diffusion of the penetrant is expected to follow the chain topology more closely. This effect can be seen in Figure 5, where the value of x approaches 0.5 as the structure densifies and the anomalous regime extends for a longer period.

Figure 6 shows the van Hove analysis for a typical structure (7 × 7 × 7 lattice, $\rho = 0.892$ g/cm^3), which is representative of all the results obtained in this study. Clearly the simple limiting law (eq 4) is not observed at any of the times examined. Further, as $t \rightarrow \infty$, the statistics for calculating $G_s(r, t)$ become very poor due to the limited data. However, from Figure 6, it can be seen that the functions can be deconvoluted into several constituary Gaussian distributions. The results show that although the measured van Hove functions are highly irregular, a linear combination of five modes produces a good fit to the data, corresponding to five distinct diffusing populations. Nearly all of the simulation results could be successfully deconvoluted to five populations.

Analysis of the van Hove functions allows for an estimate of the fraction of penetrants trapped within its initial position. This is accomplished by calculating the average distance ($\bar{r}_i$) diffused for each of the five modes as a function of time, shown in Figure 7 for a structure of $\rho = 0.892$ g/cm^3. The horizontal line indicates the threshold distance (11.3 Å in this case) used for estimating the fraction of the population that was trapped. The threshold distance was taken to be L_c, the mean free path as calculated from the VACF, so

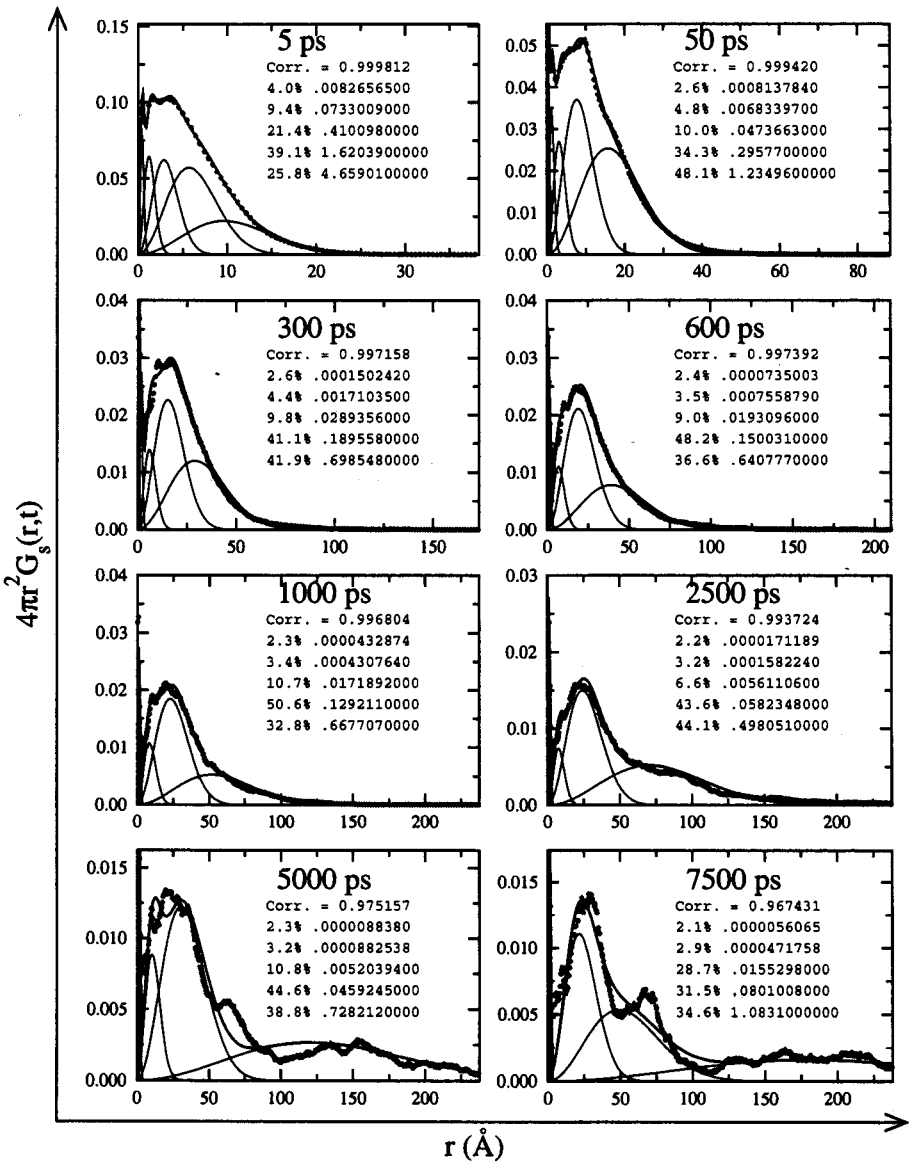

Figure 6. Analysis of van Hove functions by fitting five modes to the simulation results of diffusion in a typical 0.892 g/cm^3 polymer structure, generated from a 7 × 7 × 7 lattice. Similar results were obtained for all structures in this study. The numbers indicate the weight f_i and the diffusivity D_i associated with each of the underlying modes.

that a penetrant was considered trapped if it did not diffuse further than the mean free path after 5 ns of simulation time. For the case shown in Figure 7, it is clear that the two slower modes did not diffuse further than the threshold distance within 5 ns, and this corresponds to the trapped fraction of penetrants. The threshold time of 5 ns that was chosen was sufficient for the individual penetrants in most of the systems to reach the Fickian diffusive regime. These two modes represent trapped penetrants and constitute 5.5% of the total penetrant population. Figure 8 shows the trapped fraction found by the van Hove function analysis as a function of the specific volume of the polymer structures, for all the structures considered in this study. As the polymer densifies, an increasing fraction of the penetrant population is trapped within a local area of its initial position and fewer of the pathways percolate the simulation cell. For the highest density structure considered here, nearly half of the penetrants are trapped.

The average diffusivity as calculated from the van Hove functions, $\bar{D}_{vH}$ of He in a series of structures

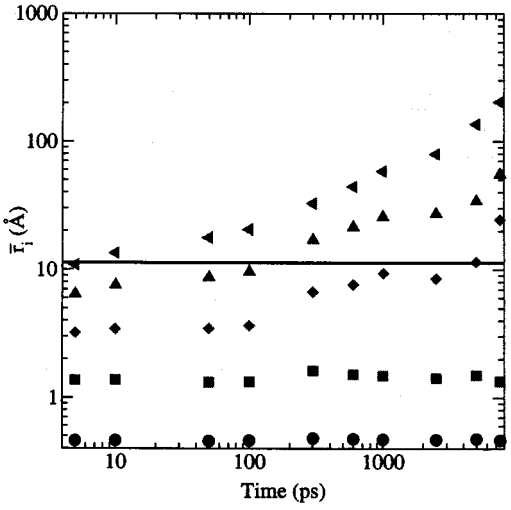

Figure 7. Average distance diffused in each mode in Figure 6 as a function of time. The horizontal line is drawn at L_c = 11.3 Å.

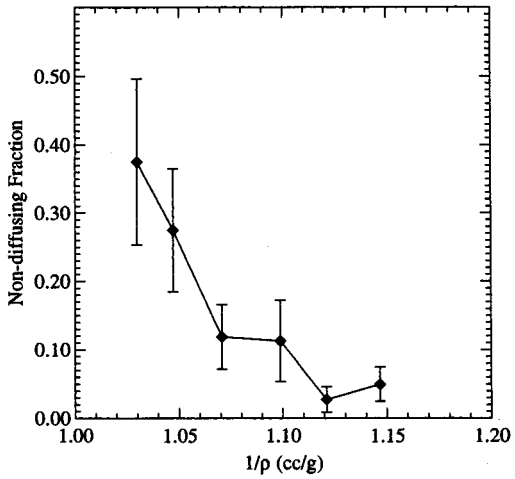

Figure 8. Average trapped fraction as a function of specific volume.

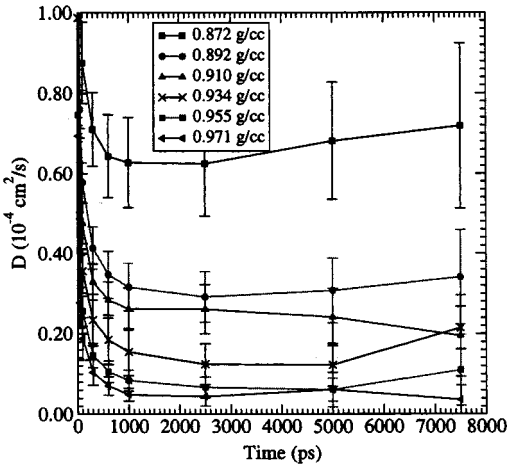

Figure 9. Average diffusivity, $\bar{D}_{vH}$ as a function of time for all structures considered. Error bars indicate one standard deviation.

(7 × 7 × 7) at varying density is shown in Figure 9. The error bars indicate the standard deviation between different structures at the same density (five statistically independent structures were examined at each density). The increase in the error bars at longer times correspond to a decrease in the amount of data available at these times. Figure 9 shows that the average instantaneous diffusivity stabilizes to within 12% of the long-time value of diffusivity by 1 ns of simulation time. This analysis allows the estimation of the diffusivity for the higher density structures where the MSD curves do not yet yield clear Fickian regimes. The overall diffusivity for each density was calculated by taking the average of the instantaneous diffusivities from 1 ns onward.

Figure 10 shows the long-time diffusivity ($\bar{D}_{vH,t\to\infty}$) as a function of the specific volume of the polymer structures, compared to the results of the MSD analysis (D_{MSD}) and the results found for Helium in a polypropylene structure where thermal motion was allowed.[5] The figure also shows the diffusivity ($\bar{D}'_{vH,t\to\infty}$) obtained after correcting for the trapped fraction of diffusants. The figure clearly shows the effect of densification of the structures on diffusion. diffusion is strongly inhibited by a reduction in the void volume in the structures (Figure 4). Correcting for the nondiffusing fraction yields values for the diffusivity within the calculation uncertainty, indicating that the reduction in diffusivity cannot

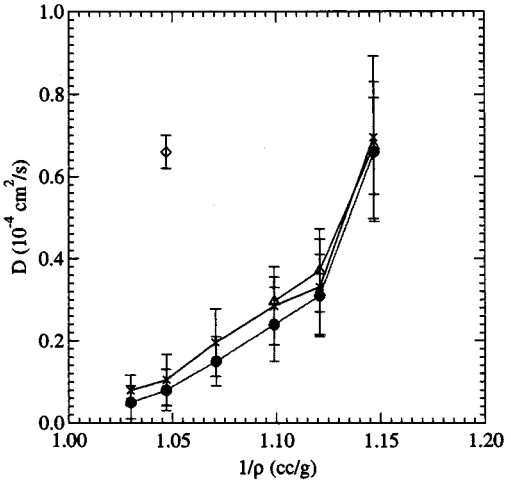

Figure 10. Diffusivity of helium in polypropylene structures as calculated by MD. $D_{vH,t\to\infty}$ (●) are from analysis of the van Hove function, ($\bar{D}'_{vH,t\to\infty}$) (×) from van Hove function analysis, after correcting for the trapped fraction, D_{MSD} (△) from analysis of the MSD's, and D (◇) from Cuthbert et al.[5] for the same polymer matrix but with thermal motion allowed.

be primarily ascribed to an increase in the number of trapped penetrants.

The effect of thermal motion on the calculated diffusivity is also evident in Figure 10 for $\rho = 0.955$ g/cm^3. Quenching polymer motion reduces the diffusivity to almost an order of magnitude lower than for the mobile matrix. This is consistent with previous comparison.[10,11] It is clear that thermal motion enhances molecular diffusion by almost an order of magnitude. This can be partially explained by the dynamic formation of new pathways, or "necks" between the tortuous cavities in the polymer structures through which penetrants can diffuse. For the mobile matrix, these jumps constitute the primary diffusion mechanism, which can be characterized as an activated process.[1] A number of studies have measured the jump distance to be of the order of 10 Å,[5,12] roughly the same size as the cavities in the polymer. In the case of the rigid polymer matrix, once the diffusion pathways are limited to the percolated pathways, the mechanism of penetrant diffusion is altered in a significant way. The direct effects of polymer topology on diffusion diminishes in the mobile matrix due to the local rearrangements leading to the dynamic formation of new diffusion pathways.

B. Diffusion Mechanism. Applying the basic theory of rate processes[29] to the self-diffusion of a penetrant in a glassy polymer membrane, the diffusivity would be described by an activated process, according to eq 9[29]

$$D = \frac{\lambda^2}{v_f^{1/3}} \bar{v} \exp\left(\frac{-\Delta E^{vap}}{nRT}\right) \tag{9}$$

where λ is the average jump length, v_f is the free vol, $\bar{v}$ is the average thermal velocity, ΔE^{vap} is the change in energy upon evaporation of a single atom from the mixture to the gas phase, and n is an empirical constant, approximately 2.45.[29] If the free volume is modeled in terms of a spherical packing of liquid molecules, v_f becomes related to the specific volume by $v_f = c^3((v^*)^{1/3} - d)^3$,[29] where c is the packing parameter, v^* is the volume per liquid molecule, related to the specific volume of the fluid, and d is the incompressible diameter of a liquid molecule. By our estimating the parameter

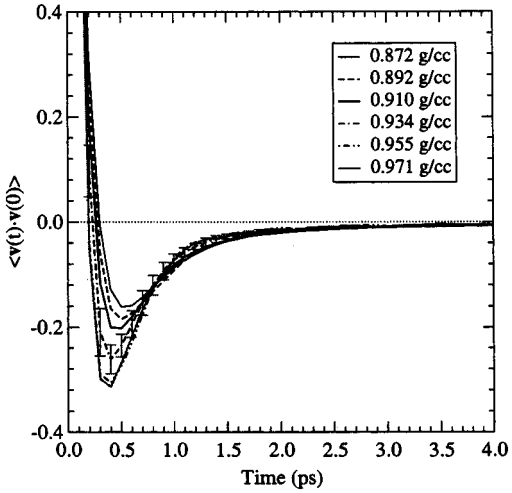

Figure 11. Average velocity autocorrelation functions for He atoms in 5 structures of each density on the $7 \times 7 \times 7$ lattice. The error bars indicate the typical standard deviation between five independent structures, for reference.

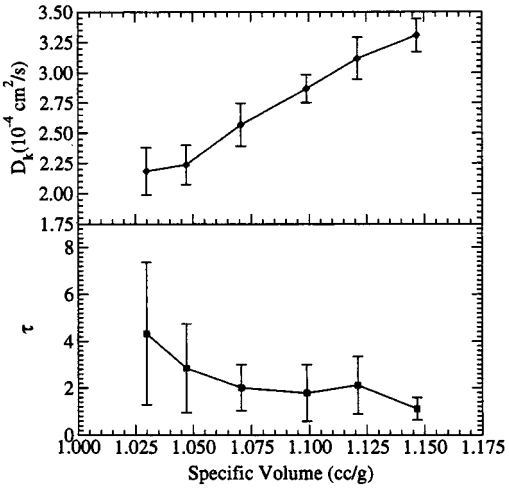

Figure 12. Kinetic diffusivity and estimated tortuosity of polymer structures as a function of polymer specific volume.

λ to be on the order of 10 Å and modeling the free volume as a liquid lattice, eq 9 qualitatively described the simulation results obtained for the diffusivity (Figure 10). However, the model failed to quantitatively predict the activation energies, yielding values an order of magnitude larger than μ^{Heex}, the calculated excess chemical potential of He in the structures. At the infinite dilution limit, one expects the excess chemical potential of He in the structures to be close to ΔE^{vap}, and the activation energies are not expected to be larger than $2.45\Delta E^{\text{vap}}$.[29]

Detailed analysis of jump maps,[7] generated for the results obtained here, showed that the dominating mechanisms of motion were not jumps between cavities. The jump maps were generated by calculating the squared distance between positional averages of the penetrant over a series of time intervals: 1, 2, 5, 10, and 20 ps. The maps were characteristic of a kinetic collisional type motion, similar to those obtained by Han and Boyd[7] for diffusion of CH_4 in the high-temperature polymer melt. No evidence was found that the mechanism of diffusion for the results obtained in this study could be described by a simple hopping mechanism between cavities in the polymer structure.

The above results are in contrast with cases where polymer motion is allowed,[1,5,7,13] for which penetrant diffusion can be described by an activated process. In the mobile matrix model, penetrants are thought to jump between cavities through a "neck". The cavities are dynamically formed and the polymer motion aids the formation of the "neck".[1,30] In contrast, for the static polymer structures studied here, diffusion is dependent on the percolation of existing pathways through the periodic polymer structure. The diffusion mechanism in the static structure is better described by an approach based on kinetic theory, similar to the dusty gas model.[31]

The average VACFs of the penetrants as a function of polymer density are shown in Figure 11. The curves are averages between five independent structures, with the typical standard deviation indicated as error bars on the 0.934 g/cm^3 line. As the polymer densifies, the time required for velocity reversal, $t|_{\langle v^{\text{acf}}\rangle=0}$, decreases. Furthermore, the decay in the VACF after velocity reversal is faster for the higher density cases than for the lower density cases. This can be explained by the diminishing void volume as the polymer densifies, forcing greater interaction between the penetrant and the polymer matrix. From the VACF, L_c was calculated to be 11.0 ± 0.1 Å for all the structures, with no density dependence within the uncertainty. This estimate for L_c agrees well with the expected cavity size for amorphous polypropylene structures of high density (0.95 g/cm^3),[5] as well as results obtained by Greenfield et al.[12] for the size of sorption macrostates in atactic polypropylene of experimental density at 233 K and 1 atm (0.892 g/cm^3). The value also agrees well with l_{c1}, the extent of local correlation in the structure.

Figure 12 shows the results for the kinetic diffusivity and tortuosity as estimated from the VACFs, using eqs 7 and 8, as a function of the specific volume of the polymer structures. The tortuosity factors obtained are reasonable and fall within the range of 3−7 expected for amorphous porous media,[32] especially when considering the low porosities. The tortuosity factor decreases as the polymer matrix expands and approaches unity for the lowest density structure considered here. It is clear that diffusion in the higher density cases is limited by the tortuous nature of the diffusion pathways, which explains the lower diffusivities in the higher density structures shown in Figure 10.

C. Simulation Box Size Effects. 1. Gas Solubility Calculations. Analyzing the calculated excess chemical potential is an effective tool to measure the effects of simulation size on the sorption sites in the polymer structure.[5,6] Figure 13 shows the distribution of the excess chemical potential as a function of the simulation box size, smoothed to account for the finite bin size. The number of insertions to measure the excess chemical potentials were equal for all four sizes, so that the differences in the data are not statistical artifacts. The distribution for $\mu^{\text{Heex}}(x_{\text{He}}\rightarrow 0)$ is sharper for the larger simulation sizes, consistent with the expectation that the relative fluctuations about the thermodynamic average decrease as a result of the larger system size. For the larger sized structures, the sorption site distribution is more representative of the population average, leading to better results for the probability distribution of the excess chemical potential. The inlay in Figure 13 shows the average values of the excess chemical potential as a function of the simulation box size, where no discernible size effects can be quantified.

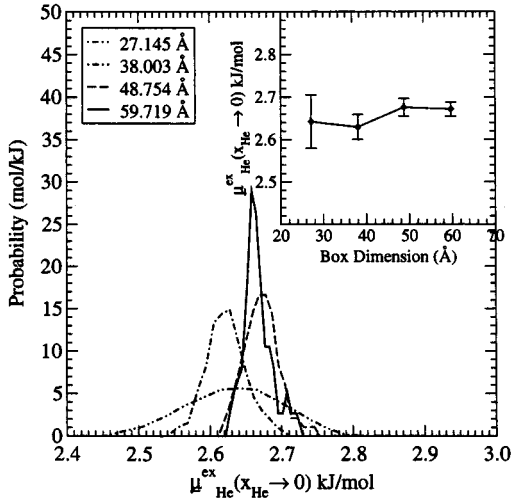

Figure 13. Distributions of excess chemical potential for He inserted into four different simulation box sizes of 0.872 g/cm^3 polypropylene, averaged over multiple structures. The inlay shows the average values of $\mu_{He}^{ex}(x_{He}\rightarrow 0)$ as a function of simulation box size.

2. Size Effects on Diffusivity. The effect of simulation box size on the diffusivity was studied by performing simulations of He in 0.872 g/cm^3 polypropylene structures ranging in linear box dimensions from about 27 to 60 Å. Comparison with the case in which the polymer was allowed thermal motion[5] enables identifying the influence of polymer motion on simulation box size effects. Figure 14B shows the diffusivity, $\bar{D}_{vH,t\rightarrow\infty}$ of helium in different sized simulation boxes as calculated from analyzing the resulting van Hove functions, as well as that obtained directly from the MSD, D_{MSD} (eq 3). The four data points were generated from the first four structures in Table 1, corresponding to a 5 × 5 × 5, 7 × 7 × 7, 9 × 9 × 9, and 11 × 11 × 11 sized lattice backbone. It is clear that, for the rigid matrix explored here, the diffusivity depends on simulation size.

The Fickian diffusivities shown in Figure 14B decrease with increasing box size. The error bars in the largest structures (based on an 11 × 11 × 11 lattice) are markedly smaller than that for the other structures. Also note the excellent agreement between the two methods of calculation for the larger structures. Also shown in Figure 14 is ($\bar{D}'_{vH,t\rightarrow\infty}$) the diffusivity after correcting for the nondiffusing fraction. ($\bar{D}'_{vH,t\rightarrow\infty}$) has the same qualitative trend as D_{MSD} and $\bar{D}_{vH,t\rightarrow\infty}$. The horizontal line shown in Figure 14B is the expected diffusivity $D_{N\rightarrow\infty}$ based on the $D \propto 1/N$ dependence[33] exhibited in the three larger structures studied here. $D_{N\rightarrow\infty}$ was found to be $0.266 \pm 0.093 \times 10^{-4}$ cm^2/s. Figure 14A shows the dependence of the nondiffusing fraction on the simulation box size. As the simulation size increases, a slight increase in the nondiffusing fraction leads to slightly lower diffusivities, indicating a reduction in the number of percolated diffusion pathways for the larger simulation sizes. This, however, is insignificant compared to the expected, statistical $D \propto 1/N$[33] relationship.

The crossover times and distances reported in Figure 14, parts C and D, were calculated by fitting two power law regimes to the MSD results. The first fit was to the anomalous regime, when $D \propto t^{0.5}$, and the second fit was through the region in the MSD where the slope is within 10% of 1.0. The crossover time was taken to be the point where these two straight lines crossed.[14] As shown in Figure 14D, the crossover distances, as defined by the intersection of the fit lines, are comparable to or longer than the linear box dimensions for the two smallest structures. This shows that the box turnover from anomalous to Fickian diffusion can be artificially induced by a small simulation box.

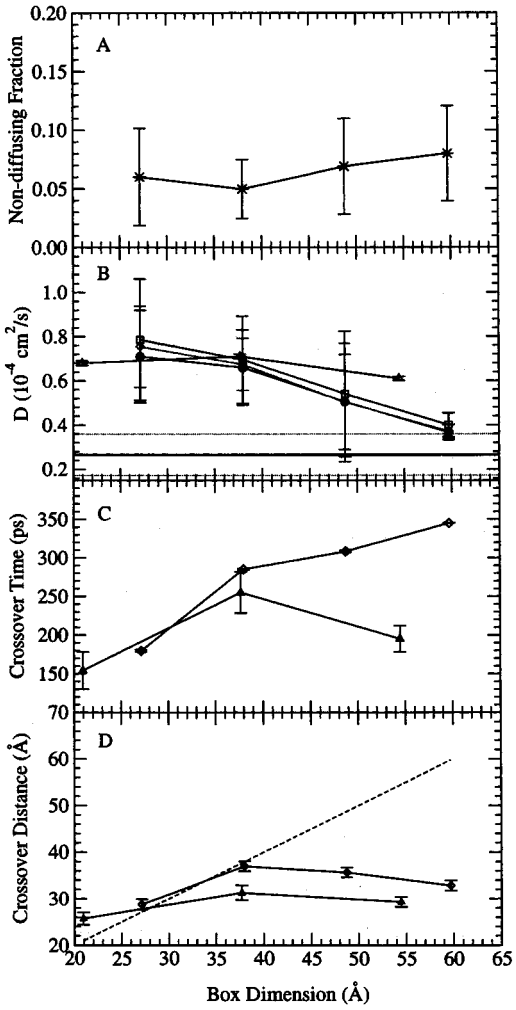

Figure 14. Comparison of simulation size effects on (A) the nondiffusing fraction (★), (B) diffusivity $\bar{D}_{vH,t\rightarrow\infty}$ (◇), D_{MSD} (●), and ($\bar{D}'_{vH,t\rightarrow\infty}$) (□) for aPP at 0.872 g/cm^3 and D (△) from Cuthbert et al.[5] for aPP at 0.95 g/cm^3, where the polymer was allowed thermal motion. (C) Crossover time and (D) distance (this work (◇) for aPP at 0.872 g/cm^3 and results from Cuthbert et al.[5] (△) for aPP at 0.95 g/cm^3). The thick horizontal line in part B at 0.266×10^{-4} cm^2/s indicates $D_{N\rightarrow\infty}$, found by extrapolation of $\bar{D}_{vH,t\rightarrow\infty}$ and D_{MSD} to $N \rightarrow \infty$, according to $D \propto 1/N$,[33] where the dotted lines indicate the uncertainty in $D_{N\rightarrow\infty}$. The dashed line in part D indicates the simulation box size.

Weber and Paul[14] determined for their lattice simulations that the critical box size (the size where the crossover distance becomes independent of the box size) was approximately 75 lattice units. The characteristic size of their monomers were 2a, where a is the lattice constant. This was also the size of the penetrant that diffused in their coarse-grained system. Each monomer defined in this manner corresponded to a piece of chemically realistic chain consisting of about five backbone bonds.[14,34,35] If the lattice size in the system studied here is taken to be the characteristic size of a He atom, the critical box size in the system studied here is about 15 units, which is a factor of 5 *smaller* than that found by Weber and Paul.[14] The different dependence on simulation box size can be ascribed to the penetrant size being significantly smaller in our work. If the polymer

were modeled as a coarse-grained chain, the He penetrants would be a factor of 3 smaller than the "monomers". The larger amount of void volume available to the smaller penetrant results in a Fickian diffusion regime that is reached much faster, i.e., shorter crossover time. See Cuthbert et al.[5] for another example of this effect.

Direct comparison to the case studied by Cuthbert et al.,[5] who simulated atactic polypropylene at $\rho = 0.95$ g/cm^3, is complicated by the fact that diffusion in the frozen matrix is greatly suppressed at this density. The time required to reach Fickian diffusion is long enough such that the crossover time is not achieved on the time scales probed here. Note, however, from Figure 10 that the diffusivity for the frozen 0.872 g/cm^3 structures are quantitatively similar to that calculated by Cuthbert et al.[5] for the mobile 0.95 g/cm^3 structures. The turnover distance is also approximately the same, as shown in Figure 14. Figure 14 also shows that the size dependence on the turnover distance is much less pronounced for the mobile polymer matrix than for the rigid matrix. Polymer motion results in suppression of simulation size effects due to the temporal evolution of the matrix. Although the turnover distance exhibits a simulation size dependence for both systems, the diffusivity is much less sensitive to simulation size for the mobile matrix. Thus, comparison between the mobile and frozen matrix systems demonstrates that polymer motion aids in mitigating the influence of periodicity on the calculated tracer diffusivity.

4. Conclusions

Suppressing polymer motion fundamentally changes the mechanism of penetrant diffusion in glassy polymers from an activated diffusion to a kinetic motion hindered by tortuosity. We have shown that anomalous diffusion in the frozen polymer matrix results from the tortuous diffusion pathways of the penetrants in the polymer structure. Through comparisons with previous studies, the anomalous regime is shown to be significantly shorter for mobile matrix polymer systems, supporting the notion that polymer motion erases some of the effects of the polymer structure on penetrant diffusion by allowing jumps between sorption states in the structure that are disallowed when the matrix is frozen. The dynamic formation of necks between cavities aids diffusion by providing shorter pathways and overcoming some of the tortuosity inherent in the polymer structure. These jumps dominate molecular motion and the mechanism of diffusion becomes activated.[1] Densification of the polymer structures results in increased tortuosity (τ) and trapped fraction (f^{trapped}), and reduces the diffusivity. This effect can be ascribed to percolated diffusion pathways in the amorphous pore network closing up as the material densifies. The dynamic behavior of the penetrant in the anomalous regime was found to be consistent with the center of mass diffusion of a reptating chain ($\langle r^2 \rangle \propto \sqrt{t}$), suggesting that in the anomalous regime the penetrant follows the local correlation along the polymer backbone. This effect is enhanced for the higher density structures.

The effects of simulation size on the calculated diffusivity become more pronounced for the frozen matrix explored here. The effect is observed most significantly for the turnover distance. Polymer motion can partially "erase" the periodicity and suppress box size effects. The correlation between the turnover distance, the box size, and diffusivity for rigid polymer matrices is illustrated for a realistic polymer structure, which shows the minimum box size required is 15 times the penetrant size, or about 10 times the monomer size, for the system considered here.

Acknowledgment. Funding for this work was provided by NSF Grant No. EEC-0085461 and DuPont through grants in the Aid to Education program. Useful discussions with Dr. Steve Lustig from DuPont are gratefully acknowledged.

References and Notes

(1) Gusev, A. A.; Müller-Plathe, F.; van Gunsteren, W. F.; Suter, U. W. *Adv. Polym. Sci.* **1994**, *116*, 209.
(2) Theodorou, D. N. *Diffusion in Polymers*; New York: Marcel Dekker, 1996.
(3) Tamai, Y.; Tanaka, PH.; Nakanishi, K. *Macromolecules* **1994**, *27*, 4498.
(4) Sok, R. M.; Berendsen, H. J. C.; Van Gunsteren, W. F. *J. Chem. Phys.* **1992**, *96*, 4699.
(5) Cuthbert, T. R.; Wagner, N. J.; Paulaitis, M. E. *Macromolecules* **1999**, *32*, 5017.
(6) Cuthbert, T. R.; Wagner, N. J.; Paulaitis, M. E. *Macromolecules* **1997**, *30*, 3058.
(7) Han, J.; Boyd, R. H. *Macromolecules* **1994**, *27*, 5365.
(8) Kotelyanskii, M.; Wagner, N. J.; Paulaitis, M. E. *Macromolecules* **1996**, *29*, 8497.
(9) Hahn, O.; Mooney, D. A.; Müller-Plathe, F.; Kremer, K. *J. Chem. Phys.* **1999**, *111*, 6061.
(10) Gusev, A. A.; Suter, U. W. *J. Chem. Phys.* **1993**, *99*, 2221.
(11) Gusev, A. A.; Suter, U. W. *J. Chem. Phys.* **1993**, *99*, 2228.
(12) Greenfield, M. L.; Theodorou, D. N. *Macromolecules* **1998**, *31*, 7068.
(13) Gray-Weale, A. A.; Henchman, R. H.; Gilbert, R. G.; Greenfield, L.; Theodorou, D. N. *Macromolecules* **1997**, *30*, 7296.
(14) Weber, H.; Paul, W. *Phys. Rev. E* **1996**, *54*, 3999.
(15) Weiner, S. J.; Kollman, P. A.; Case, D. A.; Singh, U. C.; Ghio, C.; Alagona, G.; Profeta, S.; Weiner, P. *J. Am. Chem. Soc.* **1984**, *106*, 765.
(16) Pearlman, D. A.; Case, D. A.; Caldwell, J. W.; Wilson, S. R.; Cheatham, T. E., III; Ferguson, D. M.; Seibel, G. L.; Singh, U. C.; Weiner, P. K.; Kollman, P. A. *AMBER 4.1*; University of California: San Francisco, CA, 1995.
(17) Gee, R. H.; Boyd, R. H. *J. Chem. Phys.* **1994**, *101*, 8028.
(18) Allen, M. P.; Tildesley, D. J. *Computer Simulation of Liquids*; Clarendon Press: Oxford, England, 1985.
(19) Theodorou, D. N.; Suter, U. W. *Macromolecules* **1985**, *18*, 1467.
(20) Epameinondas, L.; Forrest, B. M.; Widmann, A. H.; Suter, U. W. *J. Chem. Soc., Faraday Trans.* **1995**, *91*, 2355.
(21) Khare, R.; Paulaitis, M. E.; Lustig, S. R. *Macromolecules* **1993**, *26*, 7203.
(22) Boyd, R. H.; Pant, P. V. K. *Macromolecules* **1991**, *24*, 4078.
(23) Maeda, T. Structural Analysis of Atactic Polypropylene: A Study of the Glass Transition by X-ray Diffraction. Master's Thesis, University of Pennsylvania, Philadelphia, PA, 1987.
(24) Widom, B. *J. Chem. Phys.* **1963**, *39*, 2808.
(25) Deitrick, G. L.; Scriven, L. E.; Davis, H. T. *J. Chem. Phys.* **1989**, *90*, 2370.
(26) Kotelyanskii, M. J.; Wagner, N. J.; Paulaitis, M. E. *Comput. Theor. Polym. Sci.* **1999**, *9*, 301.
(27) Satterfield, C. N. *Mass Transfer in Heterogeneous Catalysis*; MIT Press: Cambridge, MA, 1970.
(28) Bird, R. B.; Stewart, W. E.; Lightfoot, E. N. *Transport Phenomena*, John Wiley & Sons: 1960.
(29) Glasstone, S. *The theory of rate processes: the kinetics of chemical reactions, viscosity, diffusion and electrochemical phenomena*; McGraw-Hill: New York, 1941.
(30) Greenfield, M. L.; Theodorou, D. N. *Mol. Simul.* **1997**, *19*, 329.
(31) Mason, E. A.; Malinauskas, A. P. *Gas Transport in Porous Media: The Dusty-Gas Model*; Elsevier: Amsterdam, 1983.
(32) Satterfield, C. N. *AIChE J.* **1975**, *21*, 209.
(33) Haile, J. M. *Molecular Dynamics Simulation: Elementary Methods*; Wiley: New York, 1992.
(34) Binder, K. *Monte Carlo and Molecular Dynamics Simulations in Polymer Science*; Oxford University Press: New York, 1995.
(35) Paul, W.; Pistoor, N. *Macromolecules* **1994**, *27*, 1249.

MA010255C